COMBUSTION AND EMISSION CHARACTERIZATION OF NATURAL GAS DOPED AMMONIA BURNER

***Zhiqiang Tian*[1,2]*, Lin Wang*[1*]*, Lu Han*[2]*,Songsong Zhang*[2*]*,Deli Zhang*[3]*,Yue Gao*[4]

(1.School of Mechanical and Power Engineering, Shenyang University of Chemical Technology, Shenyang, Liaoning, 110142, China;

2. Technological Innovation Department, China Special Equipment Inspection Group Co.,Ltd.,Beijing,100029,China;

3. Pressure special equipment inspection center, Liaoning Institute of Safety Science, Shenyang, Liaoning, 110004, China;

4. Monitoring and Analysis Department, Liaoning Ecological Environment Monitoring Center, Shenyang, Liaoning, 110161, China)

[*] Corresponding author; E-mail: wangl@syuct.edu.cn(Lin Wang);zhangsongsong0536@163.com(Songsong Zhang)

Abstract: Ammonia-doped natural gas combustion technology has attracted much attention because of its carbon reduction potential and fuel flexibility, but faces the dual challenges of unstable combustion due to uneven mixing in non-premixed combustion mode and the surge of NOx emission. In this study, a new cyclone doped combustor is designed through structural optimization, and the coupling mechanism of ammonia doping ratio on the flow, temperature and emission characteristics of the optimized combustor is systematically revealed. The optimized combustor synergized with the secondary air return improves the problem of slow flame speed of ammonia, and reduces the area of high-temperature zone and the peak concentration of thermal NO. The study on the effect of ammonia doping ratio shows that: with the increase of ammonia doping ratio from 0 to 0.8, the NO emission shows a non-monotonic tri-peak fluctuation, with the peak value of 757 ppmvd at Rm=0.4 and the minimum value of 445.67 ppmvd at Rm=0.6. The NO generation shows the evolution law of "promoting-suppressing-recovery", and this non-monotonicity comes from the dynamic equilibrium of fuel-type NOx and thermal-type NOx. This non-monotonicity results from the dynamic balance between fuel-based NOx and thermal NOx. The optimized combustor in this study effectively solves the problems of uneven mixing and high NOx emission level in single-stage non-premixed natural gas ammonia doped combustor, and provides a key theoretical basis for the multi-objective optimization of clean fuel doped combustor.

Key words*: Natural gas doping with ammonia; combustor; reaction kinetics; emission characterization*

1. Introduction

Hydrogen reduces CO_2 emissions in natural gas combustion but encounters industrial barriers due to high production costs, storage/transport challenges, and safety risks from its wide flammability range and low ignition energy [1,2]. Ammonia, functioning as a carbon-free fuel and hydrogen carrier, offers transitional benefits with easier synthesis, lower costs, and superior storage/transport capacity [3-5]. Its high energy density and infrastructure compatibility make ammonia-doped natural gas combustion a key research focus for sustainable clean energy solutions [6, 7].

Recent NH_3/CH_4 co-combustion studies reveal ammonia ratio effects: Khade et al.[8] using Chemkin, show that NH_3 increases reduce flame speed and adiabatic temperature. Ramos et al. [9] note minimal delays below 15% NH_3 but 300% delays above 30%. Valera-Medina et al.[10] observe flame destabilization at NH_3>0.8 and ignition failure at 0.9. While reducing carbon intensity, ammonia's combustion kinetic inhibition poses stability risks in ammonia-rich conditions.

Based on the deepened knowledge of the above combustion characteristics, researchers have further focused on the control mechanisms of pollutant generation during NH_3/CH_4 combustion. Hashemi et al.[11] found that low ammonia concentrations (<50%) increased NO emissions, while high concentrations (>50%) caused NO to first rise then decline. Du et al.[12] demonstrated non-monotonic NOx generation ("increase-decrease" pattern) at 900-1500°C under fuel-lean conditions (equivalence ratio <1). Yang et al.[13] numerically demonstrated that 10% ammonia addition in methane/air co-flow diffusion flames reduced peak soot volume fractions by 38.9% while increasing NO emissions by two orders of magnitude. Zheng et al. [14, 15] numerically explored radiation reabsorption in ammonia-blended flames. In CH_4/NH_3/air, statistical narrow-band modeling revealed nonlinear flame speed enhancement (peak 10.8% under rich conditions) through preheating-induced chemistry and radiation, while NHi-mediated pathways drove equivalence ratio-dependent NO generation, exhibiting a decrease-to-increase transition.

On the basis of theoretical mechanisms and experimental phenomena, engineering technological innovations have become the core direction for realizing efficient and low-pollution combustion of NH_3/CH_4. Kurata's team[16,17] developed a rich-fuel-poor-fuel staged combustor with a wide adaptability to the operating conditions, and through structural improvements, the NH_3 single-fuel NOx emission was successfully reduced to 337 ppm. Okafor et al.[18] used laser imaging and numerical simulations to demonstrate that optimizing the main combustion zone equivalence ratio (φ=1.30-1.35) reduces NOx emissions in CH_4-NH_3 blended fuel further to 49 ppm while achieving 99.8% combustion efficiency.

However, in single-stage non-premixed combustion, fuel-air diffusion limitations create localized lean zones and hotspots, exacerbating NOx formation despite staged combustion's suppression via rich/lean partitioning. While staged combustion effectively controls NOx through zoned fuel distribution, its complex implementation hinders industrial adaptability. The single-stage burner has the advantages of simple structure, easy installation and wide application range. To address mixing inefficiencies and NOx control in natural gas-ammonia single-stage combustors, this study proposes structural upgrades to cyclone burners: (1) repositioning secondary air jets and inlet layouts to enhance fuel-air mixing, (2) utilizing secondary air-induced high-temperature flue gas recirculation to improve ammonia's sluggish combustion characteristics, and (3) strategically cooling high-temperature zones via secondary air injection to suppress thermal NOx. Through coupled computational fluid dynamics (CFD) and chemical kinetic modeling, the research analyzes combustion performance, flow patterns, and emission profiles across varying ammonia blends. Results reveal ammonia's dual role in NOx modulation - promoting fuel-NOx formation while enabling reburning reduction pathways. The derived emission control mechanisms provide design guidelines for optimizing burner geometry and ammonia blending ratios in practical natural gas-ammonia co-firing systems.

2. Mathematical model and numerical solution method

2.1. Mathematical model

The controlling equations involved in this study mainly include the mass conservation equation, momentum conservation equation, energy conservation equation, and because of the chemical reaction, the component transport equation is also involved.

Continuity equation:

$$\frac{\partial \rho}{\partial t} + \nabla \bullet (\rho \vec{v}) = S_{\mathrm{m}} \tag{1}$$

Where ρ is the density, t is time, $\vec{v}$ is the velocity vector, S_{m} is the mass added to the continuous phase from the dispersed second phase.

Momentum equation:

$$\frac{\partial}{\partial t}(\rho \vec{v}) + \nabla \bullet (\rho \vec{v}\vec{v}) = -\nabla p + \nabla \bullet \left(\overset{=}{\tau} \right) + \overrightarrow{\rho g} + \vec{F} \tag{2}$$

Where p is the static pressure, $\overset{=}{\tau}$ is the stress tensor (described below), $\overrightarrow{\rho g}$ and $\vec{F}$ are the gravitational body force and external body forces.

Where the stress tensor is defined by the following equation:

$$\overset{=}{\tau} = \mu \left[\left(\nabla \vec{v} + \nabla \vec{v}^{T} \right) - \frac{2}{3} \nabla \bullet \vec{v} I \right] \tag{3}$$

Where μ is the molecular viscosity, I is the unit tensor, and the second term on the right hand side is the effect of volume dilation.

Energy equation:

$$\frac{\partial}{\partial t}(\rho E) + \nabla \bullet \left(\vec{v} (\rho E + p) \right) = -\nabla \bullet \left(\sum_{i} h_i J_i \right) + S_h \tag{4}$$

Where E is total energy of the unit, h_i enthalpy of component i, J_i is Diffusive flux of component i, S_h is the volumetric heat sources.

Component transport equations:

$$\frac{\partial}{\partial t}(\rho Y_i) + \nabla \bullet (\rho \vec{v} Y_i) = -\nabla \bullet J_i + R_i + S_i \tag{5}$$

Where Y_i is the content of component i, R_i is the net rate of production of species i by chemical reaction, S_i is the rate of creation by addition from the dispersed phase plus any user-defined sources.

The standard k-ε model was chosen for the turbulence equations, and the radiation was calculated using the P1 radiation model with WSGG (weighted sum of gray gas) model as:

$$q_r = -\frac{1}{3(a + \sigma_s) - C\sigma_s} \nabla G \tag{6}$$

where *a* is the absorption coefficient, σ_s is the scattering coefficient, *G* is the incident radiation, and *C* is the linear-anisotropic phase function coefficient.

Turbulence, chemical reaction interactions were modeled using the Finite-Rate/Eddy-Dissipation model, pressure-velocity coupling was performed using the SIMPLE algorithm, methane combustion was performed using a basic two-step combustion reaction, ammonia combustion was performed using a single-step ammonia combustion reaction proposed by Yang et al.[19].

Tab.1 Combustion reaction mechanism

Serial number	Chemical reaction equation	Level	Exponential factor /kmol·(m^3·s^{-1})	Activation energy /J·(kg·mol)$^{-1}$
R1	$CH_4+1.5O_2 \rightleftharpoons CO+2H_2O$	$[CH_4]^{0.7}[O_2]^{0.8}$	5.012×10^{11}	2.000×10^{8}
R2	$CO+0.5O_2 \rightleftharpoons CO_2$	$[CO]^{1.0}[O_2]^{0.25}$	2.239×10^{12}	1.700×10^{8}
R3	$NH_3+0.75O_2 \rightleftharpoons 0.5N_2+1.5H_2O$	$[NH_3]^{0.8}[O_2]^{0.8}$	2.510×10^{16}	3.138×10^{8}

Pollutants produced by combustion were predicted using the NOx pollutant model[20,21], and the specific reaction equations and parameters are shown in Tables 1 and 2. The equations are discretized using the second-order forward format.

Tab.2 The mechanism of NOx generation

Serial number	Type	Generation conditions	Chemical reaction equation
R4	Thermal NOx	High-temperature zone	$O+N_2 \rightleftharpoons NO+N$
R5			$N+O_2 \rightleftharpoons O+NO$
R6			$N+OH \rightleftharpoons H+NO$
R7	Prompt NOx	The low-temperature zone and the rich-fuel zone	$CH+N_2 \rightleftharpoons HCN+N$
R8			$N+O_2 \rightleftharpoons NO+O$
R9			$HCN+OH \rightleftharpoons CN+H_2O$
R10			$CN+O_2 \rightleftharpoons NO+CO$
R11	Fuel NOx	The fuel contains nitrogen.	$CN+O \rightleftharpoons C+NO$
R12			$NH+O_2 \rightleftharpoons NO+OH$
R13	N_2O intermediate	Low temperature, lean fuel, high pressure	$N_2+O+M \rightleftharpoons N_2O+M$
R14			$N_2O+O \rightleftharpoons 2NO$

2.2. Natural gas doped ammonia burner model

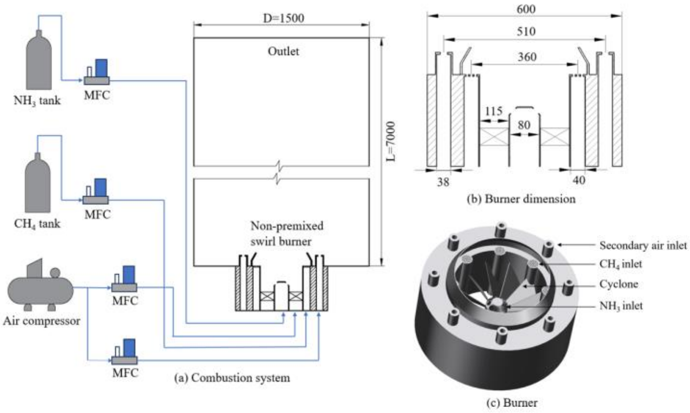

(a) Combustion system

(b) Burner dimension

(c) Burner

Fig.1 Schematic diagram of the combustion system and the size of the burner (a. Combustion system. b. Burner dimension. C. Burner)

Building upon Okafor et al.'s 50kWe micro-cyclone burner[16-18], this study reconfigured fuel inlet/swirler arrangements to address fuel-air mixing inhomogeneity and optimized secondary air inlet positioning. These adjustments enable secondary air to generate recirculation vortices, mitigating ammonia combustion stagnation while optimizing flame structure and lowering high-temperature zone temperatures. Schematic diagram of the combustion system and the size of the burner are shown in Fig.1.

2.3. Gridding and data validation

In order to carry out the grid-independence verification in the numerical simulation, this study uses different numbers of grids (1.9 million, 2.7 million, & 3.5 million) to numerically simulate the operating conditions with a heat load of 1.5MW, an ammonia doping ratio of 0.4, and an equivalence ratio of 0.9. Fig.2 shows the temperature and CO_2 volume concentration on the burner centerline versus position for different number of grids. From Fig.2, it can be seen that the difference between the simulation results of 2.7 million grids and 3.5 million grids is small. therefore, considering the computational efficiency and accuracy, 2.7 million grids are used for the ammonia-doped combustion simulation in this study. In order to verify the reliability of the model, the simulation results were compared with the experimental measurements of Ytu et al.[22], as show in Fig.3. The overall average error between the simulation and the experiment is 18.7%, The main reasons for the errors can be summarized as follows: Firstly, some experimental data points have relatively small values, causing minor changes in the simulation results to result in significant errors; Secondly, the nitrogen oxide model used is relatively simplified and fails to fully reflect the actual situation; Finally, the idealized assumptions made in the physical simulation process further exacerbate the deviation. However, this error value is within the acceptable range.

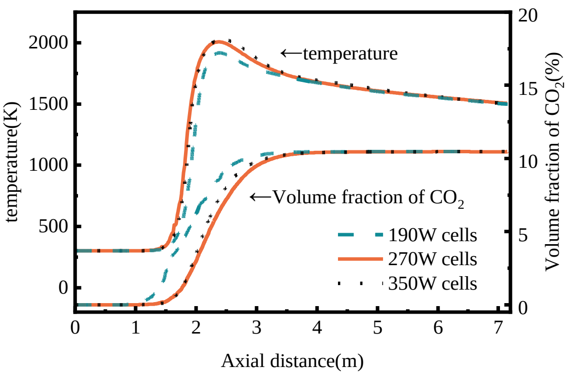

Fig.2 Mesh independence test

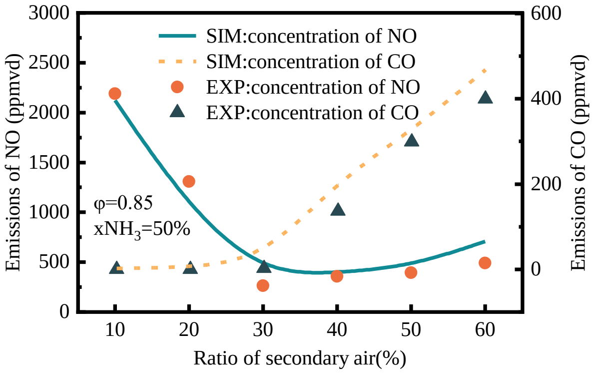

Fig.3 Data comparisons

2.4. Boundary condition

The fuel inlet are set as mass flow inlets, the fuel and air temperatures are set to 300 K.The heat load is constant at 1.5 MW for all conditions, the equivalence ratio is constant at 0.9, and the flow rate of the secondary air is constant at 20% of the total air flow rate, and the specific conditions and the values of the inlet mass flow rate are shown in Table 3, in which the dopant ratio of ammonia is Rm is indicated as:

$$Rm = \frac{Q_{NH_3}}{Q_{NH_3} + Q_{CH_4}} \tag{7}$$

Where Q_{NH_3} is mass flow of NH_3, Q_{CH_4} is mass flow of CH_4.

Tab.3 Boundary conditions under different operating conditions.

Serial number	Rm	Fuel mass flow rate/g·s^{-1}		Air mass flow rate /g·s^{-1}	
		NH_3 inlet	CH_4 inlet	cyclone	Secondary air inlet
case1	0	0	30.00	472.14	118.04
case2	0.2	7.91	27.05	465.55	116.39
case3	0.4	18.14	23.25	457.38	114.34
case4	0.6	31.87	18.16	446.50	111.63
case5	0.8	51.23	10.95	430.66	107.66

The outlet is positioned on the calculation domain's right side as a pressure outlet. Walls are classified into two types: the burner area adopts an ideal adiabatic wall surface；the combustion zone wall was set to a constant temperature of 470 K, based on the heat transfer characteristics of boiler water-cooled walls, to ideally simulate dynamic equilibrium between heat absorption and cooling water heat removal through fixed wall temperature.

2.5. The effect of optimized structure on the flow field and reaction performance of a combustor

Fig.4 shows the velocity vector distribution near the burner before and after optimization. It can be found that the velocity gradient in the central and axial flow regions of the optimized combustor is significantly reduced and the uniformity of velocity distribution is improved. The secondary combustion air is injected at the front of the combustor to enhance the synergistic effect with the cyclone air, which effectively enhances the mixing degree of fuel and air. The improved structure improves the stability of the flow field, and the optimized velocity distribution characteristics are conducive to the efficient mixing of fuel and oxidant, reducing the formation of local high temperature zones.

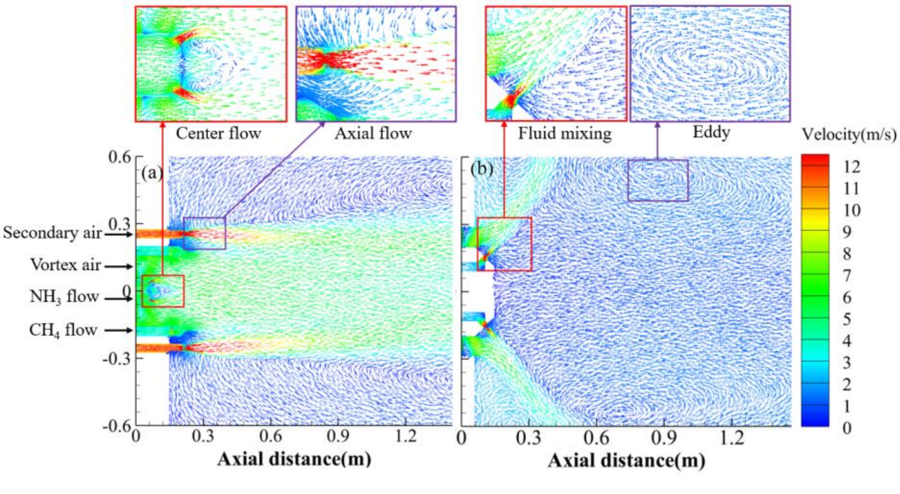

(a) The original burner. **(b) The optimized burner**

Fig.4 Axial velocity vector diagram at burner

A complete annular recirculation zone (streamline diameter: 0.3m) forms between Z=0-3m, contrasting with the original structure's divergent streamlines (max 45 degree). The optimized axial velocity gradient decreases by 50% (6→3 m/s), while the peripheral secondary airflow develops a high-speed layer that confines combustion patterns, concentrating flames and reducing high-temperature zone area.

Streamline analysis reveals the optimized secondary air inlet generates a vortex at X=0.5m cross-section, enhancing flue gas recirculation. This recirculation redirects unburned ammonia to the flame base, facilitating secondary combustion of incomplete products/pollutants while transferring heat to unignited ammonia, thereby improving flame propagation velocity. Additionally, this modification eliminates localized low-velocity dead zones caused by disordered streamline distributions in the original configuration within this region.

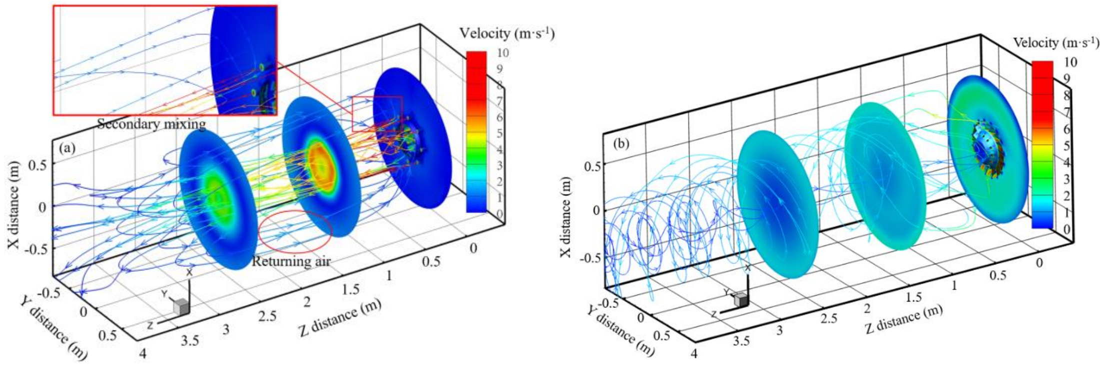

(a) Streamline diagram of the optimized burner. **(b) Streamline diagram of the original burner.**

Fig.5 Overall flow diagram of the main combustion zone

Fig.6 compares pre-/post-optimization burner temperature fields. The optimized natural gas-ammonia blend reduces high-temperature zones (1600-2000K) by 50%, forming a left-side low-temperature buffer (jet velocity > flame speed) and smoothing core gradients. These suppress thermal NOx by limiting high-temperature persistence (primary mechanism) and heat diffusion. Compared to the original configuration's large high-temperature zone (enhancing NOx formation), optimized thermal field redistribution lowers reaction driving forces while improving combustion stability.

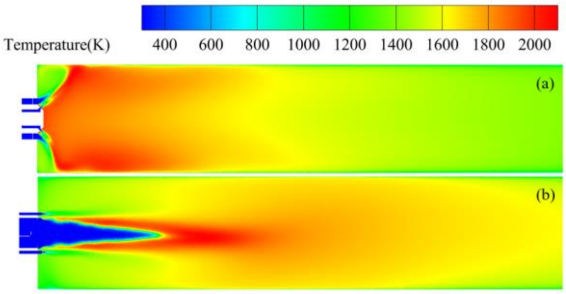

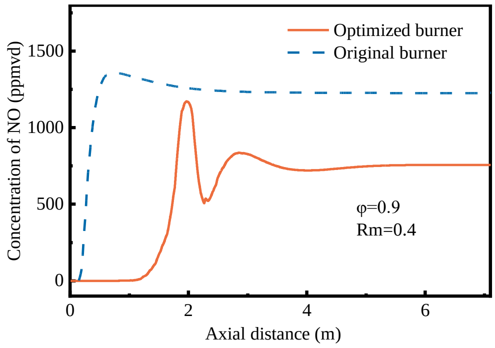

Fig.6 Temperature contrast (a. Original; b. Optimized)

Fig.7 The axial NO distribution curves contrast

Fig.7 compares NO emissions (φ=0.9, Rm=0.4) between combustor configurations. The optimized burner achieves a 13.8% reduction in peak NO (1172.6 ppmvd vs. 1360.0 ppmvd pre-optimization) within 0-2m. with peak shifted 0.3m downstream due to enhanced axial jet velocity. After stabilization, the original burner exhibited a 133.0 ppmvd NO reduction from its peak concentration, while the optimized burner achieved a 415.6 ppmvd reduction. Comparative analysis revealed a 212.5% improvement in NO suppression effectiveness of the optimized burner under identical operating conditions. The NO concentration significantly decreased in the 2.1-2.2 m interval due to unburned NH_3 reduction. Subsequently, it exhibited an initial increase followed by a decline between 2.2-3 m: the rise stemmed from concentrated fuel-NO formation in the NH_3 main combustion zone, while the subsequent reduction corresponded to secondary unburned NH_3 reduction in flue gas. Optimized exit concentration stabilizes at 757 ppmvd (38.3%

reduction). Structural improvements demonstrate dual mechanisms: delayed peak positioning and combustion-phase-modulated NO distribution, validating multistage suppression efficacy.

Secondary air inlet reconfiguration and cyclonic synergy mechanisms significantly enhanced the natural gas-ammonia combustor's performance. Optimization improved flow field stability, fuel-air mixing efficiency, and high-temperature zone reduction, effectively suppressing thermal NO. Flue gas recombustion and low-temperature buffer zones achieved full-process emission control, though fuel-type NO persisted due to ammonia doping ratios. Subsequent analysis will examine ammonia blending ratios' impacts on combustion and emission characteristics.

2.6. Effect of Ammonia Doping Ratio on Combustor Flow and Temperature Fields

Fig.8 illustrates axial velocity profiles at varying ammonia doping ratios (Rm). Based on Rm=0.4 thermal analyses, 2 m/s defines jet termination. Increasing Rm from 0 to 0.8 extends central jet penetration from 2.9m to 3.4m due to: 1) Higher fuel mass flow compensating ammonia's lower calorific value; 2) Reduced mixture density (ammonia's lower molar mass) minimizing dynamic pressure loss via Bernoulli principles; 3) Delayed thermal expansion from ammonia's lower heating value. Velocity profiles maintain shape despite mass flow increments, aligning with momentum conservation and jet stability theories.

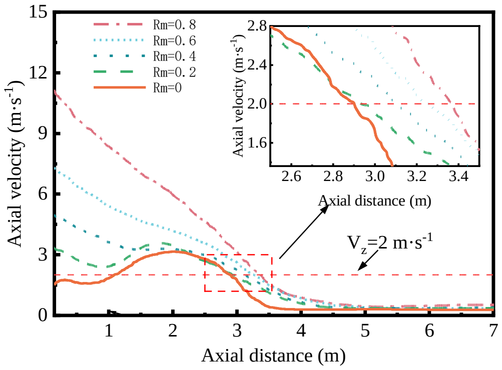

Fig.8 The depth of the central airflow jet for different Rm values

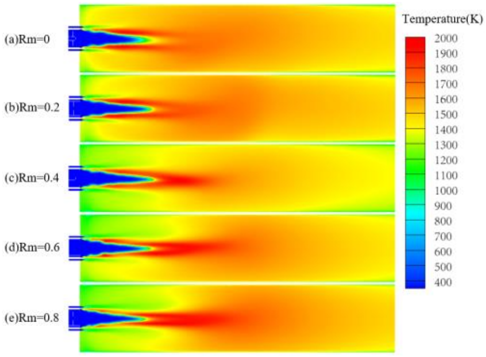

Fig.9 Temperature distribution maps for different Rm values.

Fig.9 shows temperature distributions across five ammonia blending ratios (Rm). Flame temperature peaks at Rm=0.4 via optimized airflow-enhanced mixing, then declines as NH_3's lower calorific value dominates. Flame elongation correlates with Rm through NH_3 jet rigidity (central injection), aligning with Fig.8's penetration patterns. Rm=0.6 exhibits >30% low-temperature zones (temperature < 1300K) and amplified temperature asymmetry (combustion delay/heat release inhomogeneity). Ammonia prolongs ignition delay, Large proportion of ammonia blending (flame speed < flow velocity) poses a risk of ammonia leakage caused by flameout [23,24].

Fig.10 illustrates maximum flame temperatures and turbulent kinetic energy (TKE) in the main combustion zone. At Rm=0.2/0.4, temperatures peak at 2001.7K/2063.8K with TKE=285.8/276.0 m^2/s^2, indicating robust combustion efficiency. Rm=0.6 shows minimal temperature decline (26.9K vs pure methane). Rm=0.8 exhibits poorest combustion performance with minimum values (temperature: 1895K; TKE: 210.3 m^2/s^2), demonstrating ammonia's combustion inhibition at high doping ratios.

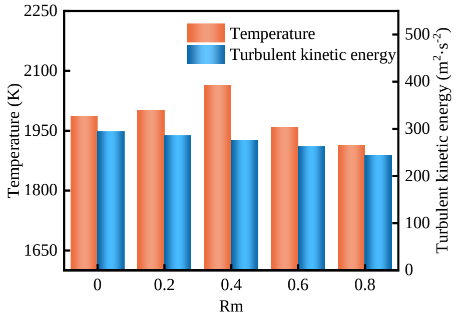

Fig. 10 The peak flame temperature and maximum turbulent kinetic energy in the main combustion zone at different Rm.

2.7. Effect of ammonia blending ratio on carbon emission and pollutant distribution

Fig.11 shows axial CO_2 volume fraction decreases with ammonia blending ratios (Rm=0→0.8). Outlet concentrations exhibit stepwise reductions: 9.46% (Rm=0.2), 21.19% (Rm=0.4), 38.32% (Rm=0.6), and 63.93% (Rm=0.8). Ammonia's carbon-free nature directly reduces carbonaceous fuel components, suppressing CO_2 generation. The linear Rm-CO_2 mitigation correlation confirms ammonia's carbon-neutral substitution potential in gas turbines through fuel decarbonization.

CO_2 reduction exhibits threshold behavior with ammonia blending ratios (Rm): limited reductions at Rm $\leqslant$ 0.4 versus $\geqslant$ 38% declines at Rm $\geqslant$ 0.6. Maintaining Rm $\geqslant$ 0.6 is critical for substantial decarbonization, with emission abatement potential progressively increasing at higher ratios, demonstrating the 0.6 threshold's importance for optimized performance.

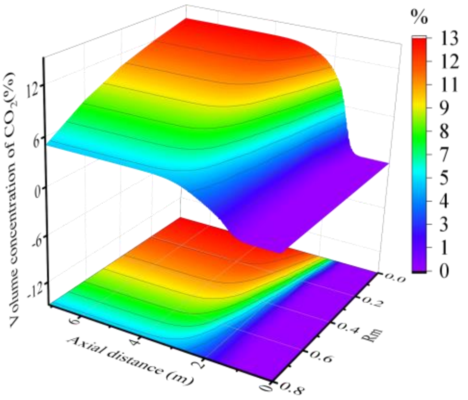

Fig.11 The volume fraction of CO_2 on the center line of different Rm furnaces

Carbonaceous fuels generate CO during incomplete combustion. Calculations reveal burner exit CO concentrations remain below 10^{-4} ppmvd across all conditions, necessitating analysis focused on the main combustion zone (Fig.12). CO emissions exhibit distinct concentration gradient patterns: increasing ammonia blending ratios progressively reduce both spatial distribution ranges and peak concentrations. At Rm=0, CO peaks at 18,226ppmvd, decreasing to 15,874 ppmvd (13.4% reduction) at Rm=0.8. This demonstrates ammonia's inhibitory effect on incomplete combustion byproducts, attributed to enhanced oxidation efficiency through optimized fuel-air mixing and thermal field homogenization under ammonia doping conditions.

CO concentration declines faster at low ammonia ratios (Rm=0-0.4), attributed to NH_3's reducing properties and optimized flame temperature regulation. Beyond Rm=0.6, CO reduction plateaus, potentially constrained by near-chemical-equilibrium combustion conditions or altered mixing efficiency. Nevertheless, high ammonia ratios maintain decreasing CO levels in the main combustion zone.

Although the addition of NH_3 to CH_4 is effective in suppressing CO_2 production and emission, it also increases the emission of the pollutant NOx. In CH_4 -NH_3 flames, the significant increase in NO is due to the addition of NH_3, and NO is mainly generated through fuel type.

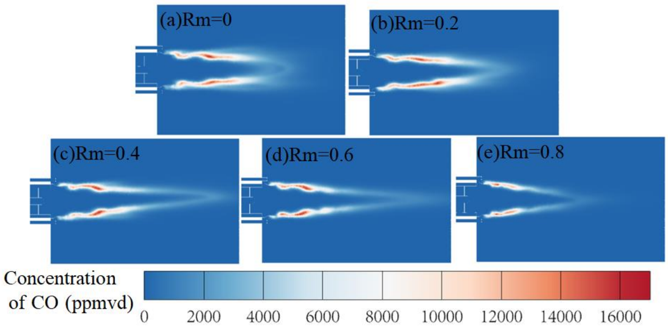

Fig. 12 Distribution of CO concentration with different Rm inn main combustion zones

Fig.13 illustrates NO/N_2O axial concentration profiles under varying Rm. NO emissions exhibit tri-peak fluctuations with increasing Rm, following an increase-decrease-increase trajectory. The outlet NO emissions concentration (757.01 ppmvd) occurs at Rm=0.4, while Rm=0.6 yields 445.67 ppmvd (19.5% above pure methane). Ammonia doping enhances fuel-nitrogen conversion but suppresses combustion temperatures, creating non-monotonic NO behavior.

Fig.13(b) shows low N_2O emissions (⩽0.63 ppmvd) across conditions. Higher N_2O levels occur at lower ammonia ratios, peaking at Rm=0.2 (0.63 ppmvd formation, 0.07 ppmvd emission). Pure methane emits 0.06 ppmvd. Emissions progressively decline with ammonia blending: Rm=0.2 (0.07)→Rm=0.8 (0.04 ppmvd). Elevated ammonia ratios thermally suppress N_2O via combustion temperature modulation.

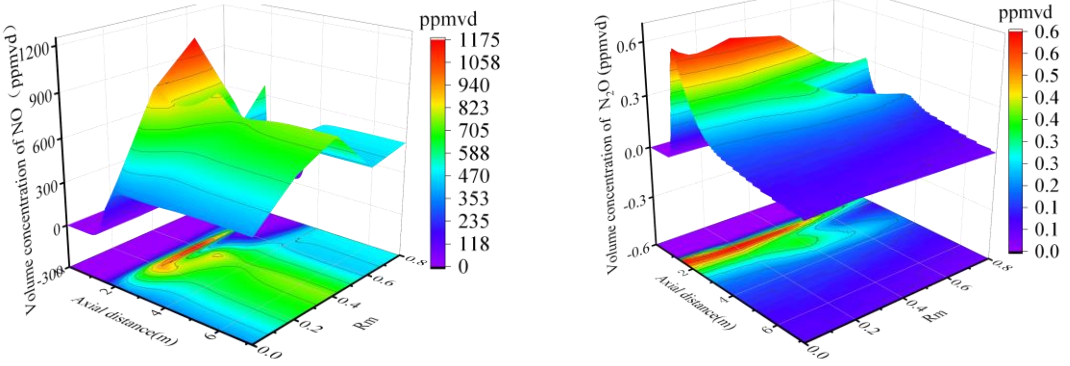

(a) NO **(b) N_2O**

Fig. 13 Contour plot of the NO and N_2O concentration in the main combustion zone of the furnace

3. Conclusion

This study investigates flow field characteristics, temperature distribution, and emission patterns in a single-stage natural gas-ammonia combustor through structural optimization using CFD and chemical kinetics. The analysis reveals intrinsic correlations between ammonia blending ratios, combustion temperature, flow structures, and pollutant emissions. and it was found that:

(1) The optimized burner enhances fuel-air mixing via secondary air optimization and cyclonic synergy. A 50% axial velocity gradient reduction forms a stable 0.3m-diameter annular recirculation zone,

eliminating 45° flow divergence. Flow homogenization reduces high-temperature area, smooths thermal gradients, and cuts thermal NO by 38.3% (1227→757 ppmvd) via localized heat mitigation.

(2) The optimized combustor extends axial jet termination (2.9→3.4m at Rm=0→0.8), driving flame reconstruction. Bernoulli effects and ammonia's low density maintain fuel momentum while reducing velocity gradients. Peripheral secondary airflow forms high-speed layers, eliminating flow disorder and dead zones. Synergistic velocity-streamline alignment matches flame propagation with jet speed to prevent blowout. Secondary air-induced flue gas recirculation enhances stability via thermal feedback.

(3) Ammonia blending ratio (Rm) critically governs emissions: CO_2 decreases 63.93% at Rm=0.8, with efficiency markedly improving at Rm⩾0.6. CO concentrations decline continuously (13.4% reduction at Rm=0.8, outlet CO-free). NO shows nonlinear trends: Rm<0.4 limits NO but insufficient decarbonization (<21%), while Rm>0.6 achieves >38% CO_2 reduction requiring stability enhancements, suggesting Rm=0.6-0.8 as the optimal carbon-nitrogen co-control window.

Acknowledgment

This work was financially supported by the project supported by "National Key R&D Program of China" (2022YFB4003904)

References

[1] Moradi R, Groth K M. Hydrogen storage and delivery: Review of the state of the art technologies and risk and reliability analysis[J]. International Journal of Hydrogen Energy, 2019, 44(23): 12254-12269.

[2] Najjar Y S H. Hydrogen safety: The road toward green technology[J]. International Journal of Hydrogen Energy, 2013, 38(25): 10716-10728.

[3] Colson S, Yamashita H, Oku K, et al. Study on the effect of injection temperature and nozzle geometry on the flashing transition of liquid ammonia spray[J]. Fuel, 2023, 348: 128612.

[4] Chu H, Yao J, Dong W, et al. Comparative effects of H_2 and NH_3 on hydrocarbon fuels laminar combustion characteristics and pollutant emissions: Status and challenges[J]. International Journal of Hydrogen Energy, 2025, 109: 129-149.

[5] Valera-Medina A, Marsh R, Runyon J, et al. Ammonia–methane combustion in tangential swirl burners for gas turbine power generation[J]. Applied Energy, 2017, 185: 1362-1371.

[6] Hasan M H, Mahlia T M I, Mofijur M, et al. A comprehensive review on the recent development of ammonia as a renewable energy carrier[J]. Energies, 2021, 14(13): 3732.

[7] Wang B, Li T, Gong F, et al. Ammonia as a green energy carrier: Electrochemical synthesis and direct ammonia fuel cell-a comprehensive review[J]. Fuel Processing Technology, 2022, 235: 107380.

[8] Khade A R, Damodara V D, CHEN D H. Reduced Mechanism for Combustion of Ammonia and Natural Gas Mixtures[J]. Clean Technologies, 2023, 5(2): 484-496.

[9] Shu B, He X, RAMOS C F, et al. Experimental and modeling study on the auto-ignition properties of ammonia/methane mixtures at elevated pressures[J]. Proceedings of the Combustion Institute, 2021, 38(1): 261-268.

[10] Valera-Medina A, Marsh R, Runyon J, et al. Ammonia–methane combustion in tangential swirl burners for gas turbine power generation[J]. Applied Energy, 2017, 185: 1362-1371.

[11] Hashemi S M, Wang P, Mao C, et al. Experimental study on the pollutant emissions of premixed ammonia/methane/air flame within porous burner[J]. Proceedings of the Institution of Mechanical Engineers, Part C: Journal of Mechanical Engineering Science, 2024, 238(9): 4139-4146.

[12] Du Y, Zong S, Wang C, et al. Study on Mechanisms of NO x Formation and Inhibition during the Combustion of NH_3/CH_4 and NH_3/CO Mixtures[J]. Applied Sciences, 2023, 13(21): 11847.

[13] Yang Y, Zheng S, Sui R, et al. Impact of ammonia addition on soot and NO/N_2O formation in methane/air co-flow diffusion flames[J]. Combustion and Flame, 2023, 247: 112483.

[14] Zheng S, He Y, Hu B, et al. Effects of radiation reabsorption on the flame speed and NO emission of NH_3/H_2/air flames at various hydrogen ratios[J]. Fuel, 2022, 327: 125176.

[15] Zheng S, He Y, Liu H, et al. Impacts of radiation reabsorption on the flame speed and NO generation of CH_4/NH_3/air flames[J]. Energy & Fuels, 2023, 37(7): 5632-5643.

[16] Kurata O, Iki N, Matsunuma T, et al. Performances and emission characteristics of NH_3-air and NH_3-CH_4-air combustion gas-turbine power generations [J]. Proceedings of the Combustion Institute, 2017, 36(3): 3351-3359.

[17] Kurata O, Iki N, Inoue T, et al. Development of a wide range-operable, rich-lean low-NOx combustor for NH_3 fuel gas-turbine power generation[J]. Proceedings of the combustion Institute, 2019, 37(4): 4587-4595.

[18] Okafor E C, Somarathne K D K A, Ratthanan R, et al. Control of NOx and other emissions in micro gas turbine combustors fuelled with mixtures of methane and ammonia[J]. Combustion and flame, 2020, 211: 406-416.

[19] Yang H M , Yeo J H , KIM N I .Optimized global reaction mechanism for H_2+NH_3+N_2 mixtures[J]. International Journal of Hydrogen Energy, 2024, 73:749-760.

[20] Bakali A E, Pillier L, Desgroux P, et al.NO prediction in natural gas flames using GDF-Kin®3.0 mechanism NCN and HCN contribution to prompt-NO formation[J]. Fuel, 2006,85(7):896-909.

[21] Miller J A, Walch S P. Prompt NO: Theoretical prediction of the high - temperature rate coefficient for CH + N→HCN + N [J]. International Journal of Chemical Kinetics, 2015,29(4): 253-9.

[22] Tu Y, Zhang H, Guiberti T F, et al. Experimental and numerical study of combustion and emission characteristics of NH_3/CH_4/air premixed swirling flames with air-staging in a model combustor[J]. Applied Energy, 2024, 367: 123370.

[23] Xiao H, Lai S, Valera‐Medina A, et al. Experimental and modeling study on ignition delay of ammonia/methane fuels[J]. International Journal of Energy Research, 2020, 44(8): 6939-6949.

[24] Dai L, Gersen S, Glarborg P, et al. Autoignition studies of NH_3/CH_4 mixtures at high pressure [J]. Combustion and Flame, 2020, 218: 19-26.

Paper submitted: 25.03.2025.

Paper revised: 19.05.2025

Paper:a accepted: 24.05.2025.